IEEE Access
Multidisciplinary | Rapid Review | Open Access Journal

Received May 22, 2018, accepted June 19, 2018, date of publication July 5, 2018, date of current version July 30, 2018.

Digital Object Identifier 10.1109/ACCESS.2018.2853166

Rotary-Percussive Ultrasonic Drill: An Effective Subsurface Penetrating Tool for Minor Planet Exploration

YINCHAO WANG[1], QIQUAN QUAN[1], (Member, IEEE), HONGYING YU[1], DEEN BAI[1], HE LI[2], AND ZONGQUAN DENG[1]

[1]State Key Laboratory of Robotics and System, Harbin Institute of Technology, Harbin 150001, China
[2]College of Mechanical and Electronic Engineering, Shandong University of Science and Technology, Qingdao 266590, China

Corresponding author: Qiquan Quan (quanqiquan@hit.edu.cn)

This work was supported in part by the National Natural Science Foundation of China under Grant 61403106, in part by the Program of Introducing Talents of Discipline to Universities under Grant B07018, and in part by the National Natural Science Foundation of China under Grant 51521003.

ABSTRACT Compared with conventional drill, an ultrasonic drill can break into rocks under lower weight on bit and lower power, which is more suitable to sample in low gravity environment for deep-space exploration. However, the ultrasonic drill cannot remove rock cuttings effectively when drilling into a certain depth. This paper proposed a rotary-percussive ultrasonic drill (RPUD), which depends on a single piezoelectric transducer to produce rotary-percussive moment to drill into rocks and remove cuttings. The RPUD consists of four parts: a piezo-ceramics, a percussive unit, a rotary unit, and a drill tool. Percussive unit magnifies the longitudinal vibration of one side of piezo-ceramics, and delivers percussive motion to the drill tool. Rotary unit transfers the longitudinal vibration of the other side of piezo-ceramics into longitudinal-torsional vibration to drive the drill tool to rotate. Percussive motion and rotary motion of drill tools are relatively independent, and thus their parameters can be adjusted separately. Finite element method is adopted to assist the design of the RPUD. Modal analysis is employed to tune the resonance frequencies of the percussive unit and rotary unit to be close. After the fabrication of a RPUD prototype, contrastive test of rotary percussive drilling and percussive drilling was carried out based on the RPUD prototype. Test results show that the RPUD can drill into the rocks and improve the efficiency of cutting removal.

INDEX TERMS Planetary rock sampling, ultrasonic drill, single piezo-ceramics, rotary-percussive drilling, drilling experiment.

I. INTRODUCTION

In recent years, minor planet exploration has become a very attractive field. Studying the geological information about minor planet contributes to understand the evolution process of the solar system. With the development of detection technology, minor planet exploration has been changed from early simple camera surface observation to landing in situ detection and sampling return [1]–[3]. According to the differences of sampling methods, detection of minor planet can be classified into three types: flying-collection (Stardust) [4], impact-collection (MUSES-C, Deep Impact) [5], [6], and drilling-collection (Rosetta) [7]. Compared with the other two kinds, drilling-collection can obtain samples on a particular location for sample return or in-situ analysis, which is widely used in existing probes. Nowadays, drilling-collection tools on the existing probes still rely on conventional rotary drills which are driven by electromagnetic motors. However, the need of weight on bit and holding torque is generally increased with the increase of drilling depth during drilling process. It is difficult to meet these requirements of conventional rotary drills by the probes under limited energy, especially on low-gravity minor planets.

Extensive researches show that [8], [9], as an attractive solution for planetary explorations, ultrasonic drills can break into rocks under low power and weight on bit, exhibit good tolerance to a wide range of temperature and do not have electromagnetic radiation. Based on the differences of working priciples, ultrasonic drills can be divided into two categories: hammer drills and rotary-hammer drills. Hammer drills can also be split into longitudinal hammer

2169-3536 © 2018 IEEE. Translations and content mining are permitted for academic research only.
Personal use is also permitted, but republication/redistribution requires IEEE permission.
See http://www.ieee.org/publications_standards/publications/rights/index.html for more information.

drills and longitudinal-torsional hammer drills. Longitudinal hammer ultrasonic drills utilize longitudinal vibration of drill bit to break rocks, such as Ultrasonic/Sonic Driller/Corer (USDC) [10], Ultrasonic Drill Tools (UDT) [11], and Ultrasonic Planetary Sample Retrieval Tool [12].

USDC is the most representative of longitudinal hammer ultrasonic drills, and it mainly has four parts: piezoelectric transducer, tuned horn, free mass, and drill tool. After being excited by resonance voltage, piezoelectric transducer generates longitudinal vibration. The vibration is amplified by tuned horn, delivered to drill tool through free mass which transforms the longitudinal vibration energy into impact motion. Rocks break when fatigue strength is ultimately exceeded by hammering. USDC can quickly penetrate into rocks with low weight on bit. Drill tool can remove a small amount of cuttings relying on the longitudinal vibration. However, when drill reaches a certain depth, it is difficult to remove the cuttings timely, which reduces drilling efficiency. Compared with longitudinal hammer ultrasonic drills, longitudinal-torsional hammer drills, which use a horn to translate the longitudinal vibration into longitudinal-torsional vibration, show a better performance at rocks broken and cuttings removal [13], [14]. However, the improvement of drilling by longitudinal-torsional vibration is still limited, and the cuttings removal efficiency still needs to be improved.

Rotary-hammer ultrasonic drills employ a drill tool with helical auger under rotary-hammer motion to break rocks and remove cuttings [15]. Compared with fluids and gas, auger removal cuttings can reduce the possibility of contamination of sample and do not require additional storage device for fluids or gas, which is more suitable for sampling in space exploration. Rotary-hammer ultrasonic drills can be classified into two types: motor-driven rotary drills and piezo-driven rotary drills. Motor-driven rotary-hammer ultrasonic drills use an electromagnetic motor as power source of rotary motion such as PARoD [16], UPCD [17], and Auto-Gopher [18]. As electromagnetic motor rotates the drill tool to remove cuttings via helical angers, drilling efficiency is improved effectively by the motor rotation. However, addition of electromagnetic motor may minify range of drilling system temperature tolerance, and adding a set of motor system to ultrasonic drills increased the degree of drilling system complexity as well.

Piezo-driven rotary-hammer ultrasonic drills employ piezoelectric transducer as the only power of rotary and hammer motions, such as SPaRH [19]. Compared with motor-driven rotary-hammer ultrasonic drills, piezo-driven rotary-hammer ultrasonic drills have an more compact structure, with lower power consumption requirements. SPaRH is made up of four parts: piezoelectric transducer, grooved horn, keyed free mass, and drill tool. Longitudinal vibration produced by piezoelectric transducer is transferred into longitudinal-torsional vibration and delivered the vibration to free mass. Then, free mass drives drill tool to realize rotary-hammer motion, which makes the rotary motion and hammer motion coupling together as well. However, with the increases demand of rotating torque, the pretightening force between the free mass and drill tool is also increased. As the rotary motion and hammer motion coupling together, the increasing of pretightening force might lead to reduction of hammer energy between free mass and drill tool, which limits the hammer motion.

It is well known that piezo-ceramics delivers the vibration energy to both sides when excited by exciting voltage. However, the existing ultrasonic drills only employ longitudinal vibration on one side to break rocks. Part of vibration energy on the other side is still not utilized. Therefore, a Rotary-Percussive Ultrasonic Drill (RPUD) is proposed, which achieves rotary-percussive motion based on the vibration energy on both sides of piezo-ceramics. To ensure that RPUD can achieve percussive motion and rotation motion synchronously, the resonance frequencies of two vibration modes are tuned to be close by finite element method. Based on the fabrication of a prototype, the vibration characteristics and drilling performance are investigated through tests.

The remainder of this paper is organized as follows. Section II introduces the working principle of RPUD. Structure design of RPUD is presented in Section III. In Section IV, the vibration displacements and rotary speed of RPUD prototype are measured. Drilling experiments are conducted to evaluate drilling performance in Section V. Finally, Section VI concludes this paper.

II. WORKING PRINCIPLE

Based on the principle of inverse piezoelectric effect, piezo-ceramics generate longitudinal vibration on both sides after stimulated by an exciting voltage. RPUD converts one side of longitudinal vibration into rotary motion and the other side into percussive motion.

The RPUD mainly consists of piezo-ceramics, rotary unit, percussive unit, drill tool, and housing, as shown in Fig. 1. Piezo-ceramics is made up of four PZT ceramics in a bolt-clamped structure and placed between rotary unit and percussive unit. Four PZT ceramics are polarized along their thickness directions, which use d_{33} mode for the excitations of longitudinal vibration to make the stress and poling directions of the PZT elements coincide. On one side, rotary unit, which connects with the back surface of piezo-ceramics, transforms the longitudinal vibration into rotary motion of the drill tool. ω is rotary angular velocity. On the other side, percussive unit, which links to the front surface of piezo-ceramics, transfers the longitudinal vibration into percussive motion of the drill tool. V is the velocity of percussive horn, and v is the velocity of drill tool. Drill tool is a tool for rock sampling with a spiral groove for cutting removal, and housing provides support for the RPUD.

Detailed working process of rotary unit and percussive unit is shown in Fig. 2. Rotary unit is composed of V type of longitudinal-torsional vibration coupling element (V-LT coupler) [20], rotor, and preload spring. Percussive unit consists of percussive horn, free mass, and storing spring. Excited by exciting voltage, piezo-ceramics transmits the longitudinal vibration simultaneously to the rotary unit and the percussive

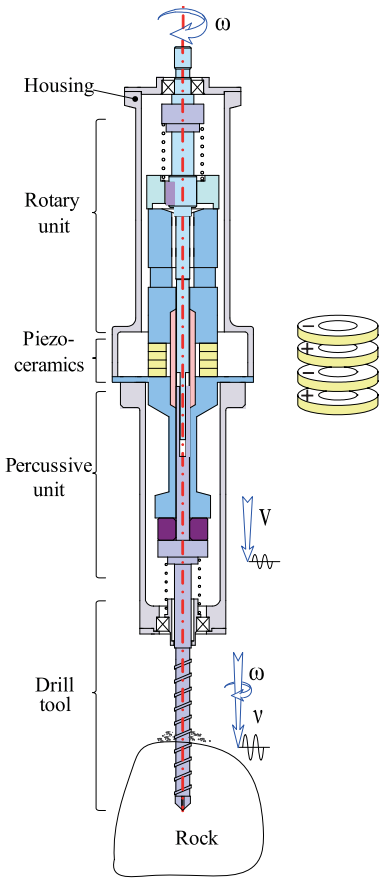

FIGURE 1. Composition schematic diagram of RPUD.

unit, as shown in Fig. 2(a). The V-LT coupler of rotary unit converts the longitudinal vibration into longitudinal-torsional vibration, formed an elliptic trajectory on the top of V-LT coupler. Depending on the preload force provided by preload spring, V-LT coupler drives the rotor to rotate continuously by friction on the contact surface. Meanwhile, the percussive horn of percussive unit amplifies the longitudinal vibration and transmits it to the free mass. Then, free mass delivers the longitudinal vibration to the drill tool causing percussive motion. Parameters of rotary motion and percussive motion can be individually adjusted without interference. As the exciting voltage on piezo-ceramics changes in sinusoidal signal cyclical, rotary unit and percussive unit of RPUD carry out periodic movement as well, which follows the sequence of (a)-(b)-(c)-(d)-(e).

III. STRUCTURE DESIGN

To achieve the rotary motion and the percussive motion working synchronously, rotary unit and percussive unit of the rotary-percussive actuator should have the same resonance frequency [21]–[24]. Finite element method is employed to adjust the resonant frequency to be the same. Finite element models of rotary unit and percussive unit are set up by ANASYS 12.0. The main structural parameters of the rotary-percussive actuator are shown in Fig. 3. Material of piezo-ceramics is PZT-82, and outer diameter is 25 mm, inner diameter is 12 mm, and thickness is 3 mm. So, the outer diameter $D_4 = 25$ mm, and length of the piezo-ceramics $L_6 = 12$ mm. These two parameters are fixed values which cannot be modified.

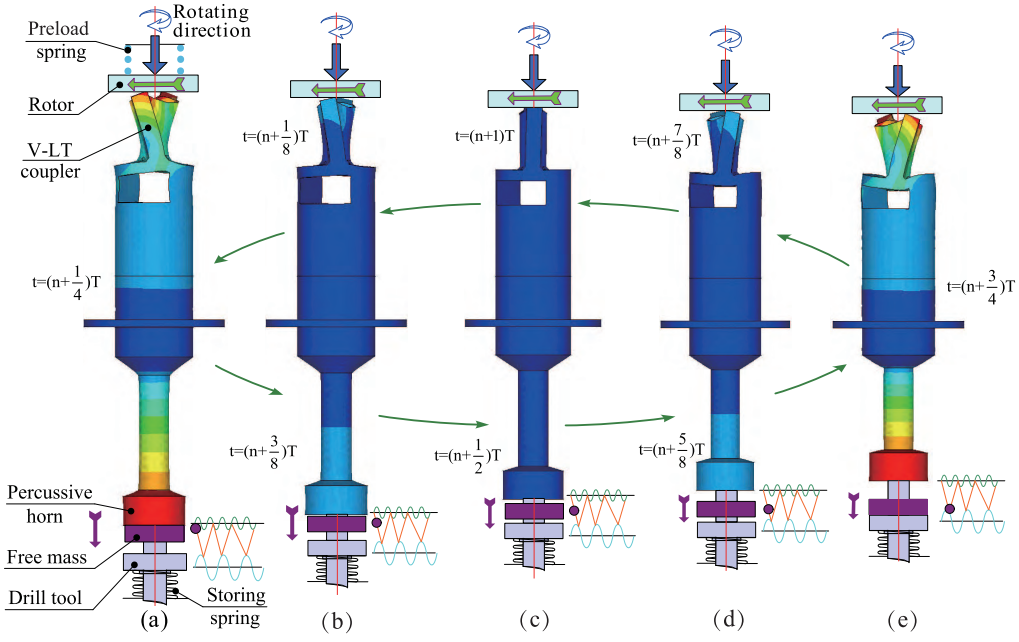

FIGURE 2. Working principle of rotary-percussive actuator.

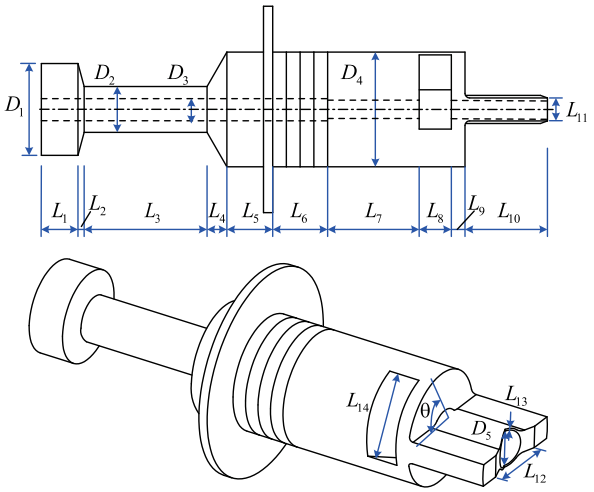

FIGURE 3. Structural parameters of the rotary-percussive transducer.

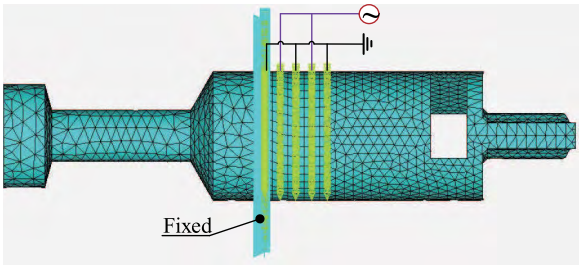

FIGURE 4. Finite element model of the rotary-percussive transducer.

A. PARAMETER DESIGN

The rest model parameters are given initial values to establish an initially finite element model of the rotary-percussive actuator, as shown in Fig. 4. The effects of resonant frequency are calculated by changing the value of each parameter through ANASYS. Fig. 5 shows the parameter changing rate of the rotary-percussive actuator. It can be seen that the parameters of and on rotary unit and on rotary unit have a big effect on the resonance frequency of the rotary-percussive actuator.

The rotary unit and the percussive unit operate simultaneously in the resonant state under the same resonance frequency by adjusting the parameters appropriately, as shown in Fig. 6(a). Vibration displacements of rotary unit and percussive unit get to the maximum value when the rotary-percussive composition works at resonant state, which indicates that rotary unit and percussive unit have achieved good matching, as shown in Fig. 6(b). The adjusted resonance frequency of the rotary-percussive actuator is 20.050 kHz.

B. WORKING FREQUENCY CALCULATION

Based on the determination parameters of transducer, working frequency is calculated to achieve good vibration effect of RPUD transducer. To accurately predict the working frequency and impedance of the RPUD transducer, the acoustic

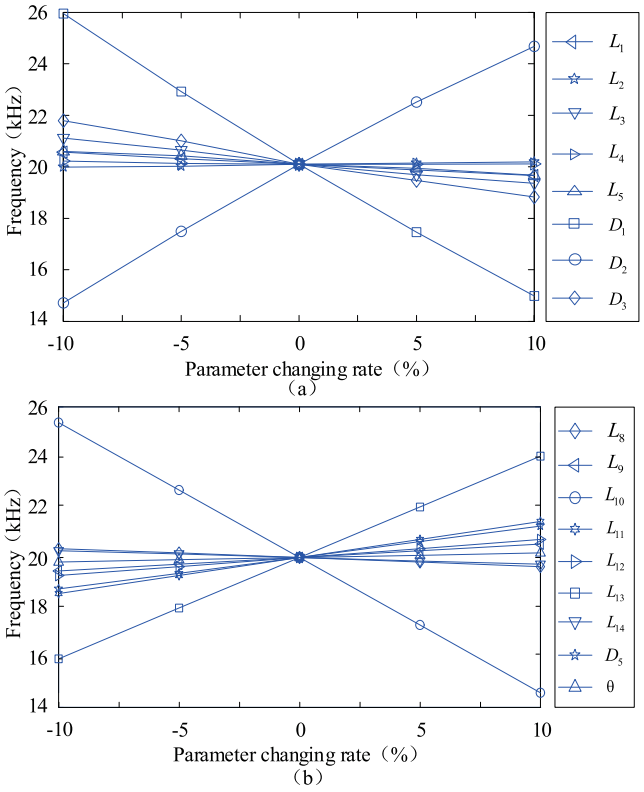

FIGURE 5. Parameter changing rate of the rotary-percussive transducer. (a) Parameter changing rate of the percussive unit. (b) Parameter changing rate of the rotary unit.

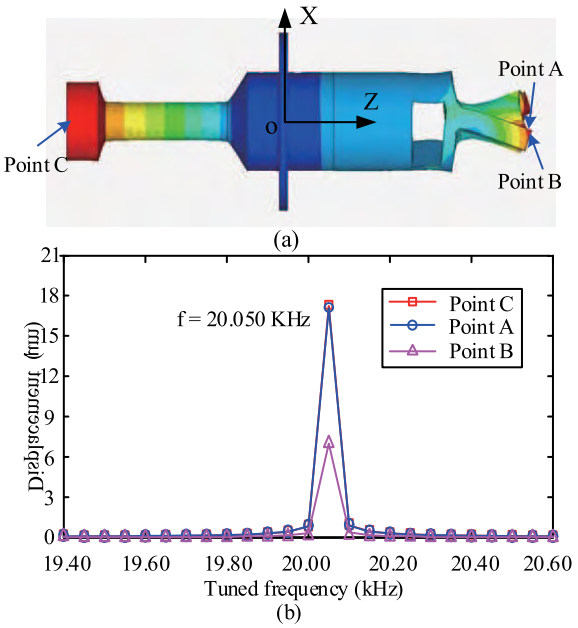

FIGURE 6. Finite element method analysis of rotary-percussive transducer. (a) Vibration modes of rotary-percussive transducer. (b) Harmonic response analysis of rotary-percussive transducer.

impedance network model of the RPUD transducer is built on the basis of the force electroacoustic analogy method [25].

The total acoustic impedance of the transducer is the sum of the acoustic impedance of the three parts of the percussive

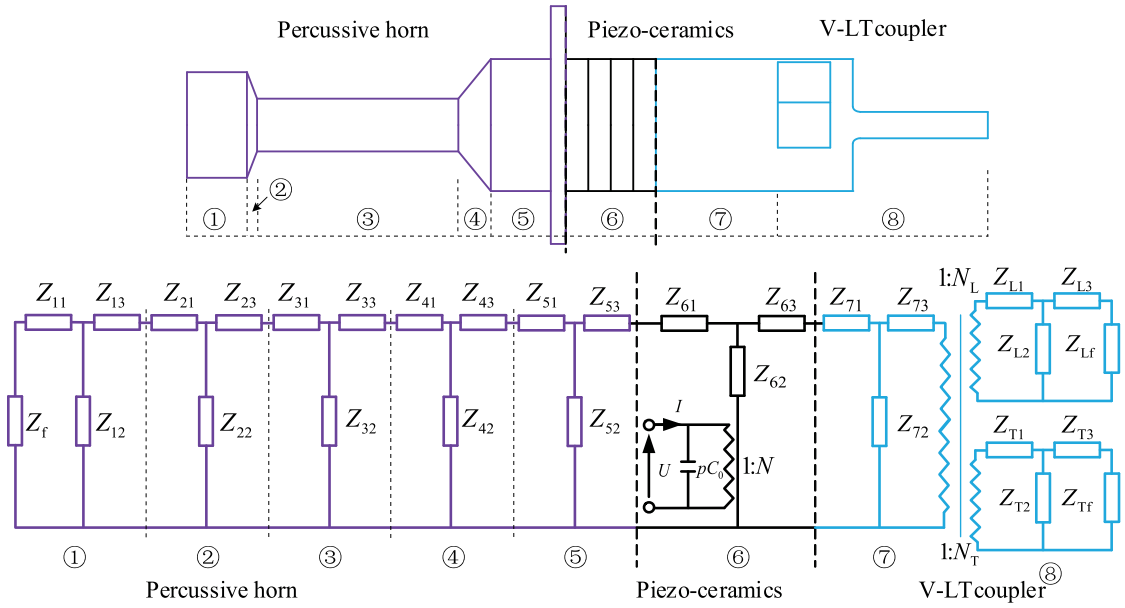

FIGURE 7. Acoustic impedance network model of RPUD transducer.

horn, the V-LT coupler, and the piezoelectric ceramics, as shown in Fig. 7. Each part of the structure impedance can be equivalent to a "T" electrical network. First, the equivalent impedance of each "T" electrical network is obtained. Then, the acoustic impedance network model of the RPUD transducer can be obtained by connecting the acoustic impedance of each part together.

The expression of the acoustic impedance of the RPUD transducer in the model is

$$\begin{cases} Z_{m1} = j\rho_m c_m S_m \tan\left(\dfrac{k_m l_m}{2}\right) \\ Z_{m2} = \rho_m c_m S_m \left(\dfrac{1}{j\sin k_m l_m}\right) \\ Z_{m3} = j\rho_m c_m S_m \tan\left(\dfrac{k_m l_m}{2}\right) \end{cases} \tag{1}$$

$$\begin{cases} Z_{n1} = -j\rho_n c_n \left[\dfrac{S_{n-1}\left(\sqrt{\dfrac{S_{n+1}}{S_{n-1}}} - 1\right) + \dfrac{S_{n-1}}{\tan k_n l_n}}{-\dfrac{\sqrt{S_{n-1}S_{n+1}}}{\sin k_n l_n}} \right] \\ Z_{n2} = -j\rho_n c_n \dfrac{\sqrt{S_{n-1}S_{h(n+1)}}}{\sin k_n l_n} \\ Z_{n3} = -j\rho_n c_n \left[\dfrac{S_{n+1}\left(\sqrt{\dfrac{S_{n+1}}{S_{n-1}}} - 1\right) + \dfrac{S_{n-1}}{\tan k_n l_n}}{-\dfrac{\sqrt{S_{n-1}S_{n+1}}}{\sin k_n l_n}} \right] \end{cases} \tag{2}$$

Where ρ_m, c_m, S_m, k_m, and ρ_n, c_n, S_n, k_n are the average density, average wave velocity, cross section area, wave number, and characteristic length of paragraph m or n respectively. In particular, $m = 1, 3, 5, 6, 7$ and $n = 2, 4$. When calculating the acoustic impedance of percussive horn, the change of wave resistance is small and continuous transition can ignore the influence of chamfer.

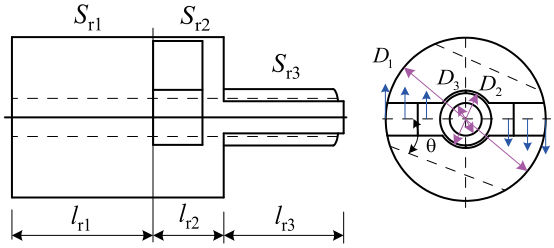

FIGURE 8. Structure of V-LT coupler.

As shown in Fig. 8, the V-LT coupler transforms longitudinal vibration into longitudinal-torsional vibration and drives the drilling tool to rotate.

The expression of the acoustic impedance of the V-LT coupler in the model is made of two parts. The longitudinal vibration part is

$$\begin{cases} Z_{L1} = -j\rho_8 c_8 \left(\dfrac{S_{r3}}{\tan k_8 l_{r3}} - \dfrac{\sqrt{S_{r2}S_{r3}}}{\sin k_8 l_{r3}} \right) \\ Z_{L2} = -j\rho_8 c_8 \dfrac{\sqrt{S_{r2}S_{r3}}}{\sin k_8 l_{r3}} \\ Z_{L3} = -j\rho_8 c_8 \left(\dfrac{S_{r3}}{\tan k_8 l_{r3}} - \dfrac{\sqrt{S_{r2}S_{r3}}}{\sin k_8 l_{r3}} \right) \end{cases} \tag{3}$$

Where ρ_8, c_8, k_8 are average density, average wave velocity, wave number respectively. S_{r1}, S_{r2}, S_{r3}, l_{r3}, l_{r3}, l_{r3} are cross section area and characteristic length of V-LT coupler.

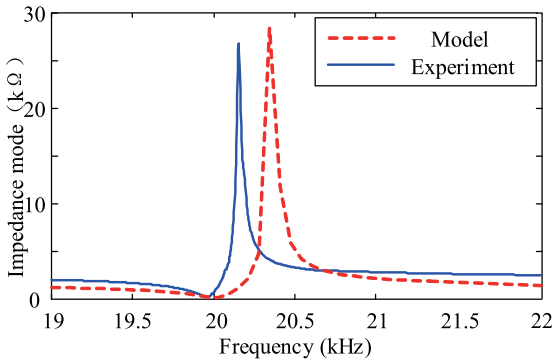

FIGURE 9. Theoretical and testing values of RPUD transducer's acoustic impedance.

And the torsional vibration is

$$\begin{cases} Z_{T1} = -j\rho_8 c_8 I_Z \tan\dfrac{k_8 l_{r3}}{2} \\ Z_{T2} = -j\rho_8 c_8 I_Z \dfrac{1}{\sin k_8 l_{r3}} \\ Z_{T3} = -j\rho_8 c_8 I_Z \tan\dfrac{k_8 l_{r3}}{2} \end{cases} \tag{4}$$

Where I_Z is the moment of inertia of the curved cross section relative to the neutral Z axis. The expression is $I_Z = \iint_S x^2 \mathrm{dS}$.

The acoustic impedance of each part is substituted into the equivalent network model. The total acoustic impedance of the ultrasonic transducer can be obtained. The impedance modulus varies with the frequency curve, as shown in the dotted line in Fig. 9. The minimum impedance frequency of the ultrasonic transducer is 20.050 kHz, and the maximum impedance mode is 28.640 kΩ. Impedance analyzer E4990A(KEYSIGHT) is used to test the acoustic impedance of the designed ultrasonic transducer prototype, and the actual impedance mode curve of the prototype can be obtained. As shown in the solid line in Fig. 9, the actual minimum impedance frequency of the ultrasonic transducer is about 19.980 kHz, and the actual maximum impedance modulus is about 26.790 kΩ.

The comparison results show that the error of working frequency is 0.35%, and the impedance mode error is 6.9%. The size of the transducer impedance mode directly affects the impedance matching between the transducer and the excitation source, which affects the output power of the excitation source. The main cause of the error are the influence of the electrode layer and adhesive, material parameters and structural dimension error on the acoustic impedance of the transducer.

C. STRUCTURE DESIGN OF RPUD

The proposed RPUD is designed based on the resonance structure parameters of rotary unit and percussive unit, as shown in Fig. 10. The bolt connects the V-LT coupler and the percussive horn with the piezo-ceramics, which provides preload stress.

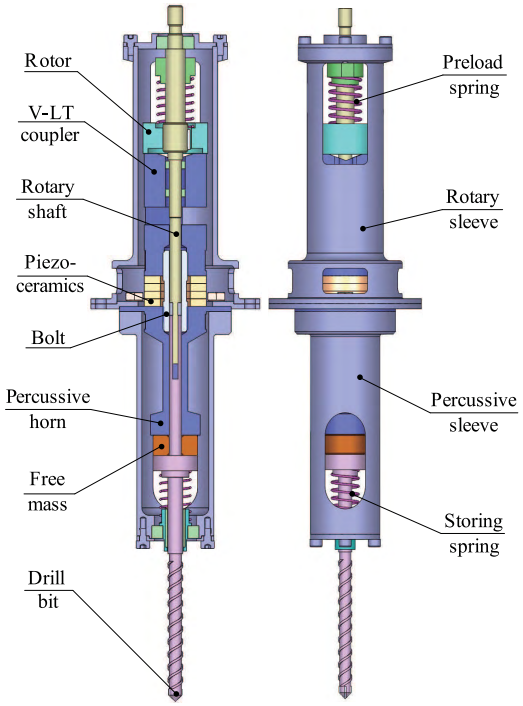

FIGURE 10. Theoretical and testing values of RPUD transducer's acoustic impedance.

In rotary unit, V-LT coupler contacts with rotor, and preload force is provided by the preload spring. Material of V-LT coupler is stainless steel and rotor is alloy steel. The contact surface of V-LT coupler and rotor is polished to improve rotary driving performance [26]. Rotor delivers the rotary motion to the rotary shaft using a key, and then rotary shaft drives drill tool to rotate. Rotary sleeve provides support for the rotary unit, and the material is aluminum alloy. In percussive unit, percussive horn contacts with free mass and drill tool, and storing spring supplies storing force. Material of percussive is stainless steel and free mass is alloy steel. In order to raise the percussive driving performance, free mass uses a unitary cylindrical structure [27], [28], material is steel and weight is 8 g.

The RPUD prototype is fabricated as shown in Fig. 11. Drill tool is a commercial Bosch multi-function drill with carbide drill bit, which is suitable for crushing rock under

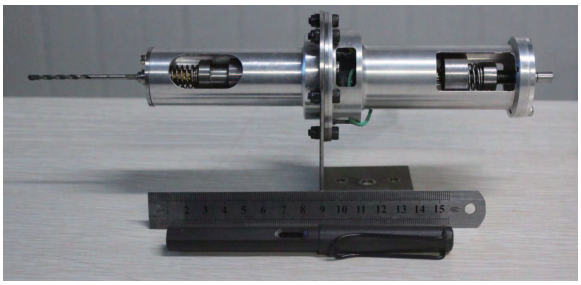

FIGURE 11. Theoretical and testing values of RPUD transducer's acoustic impedance.

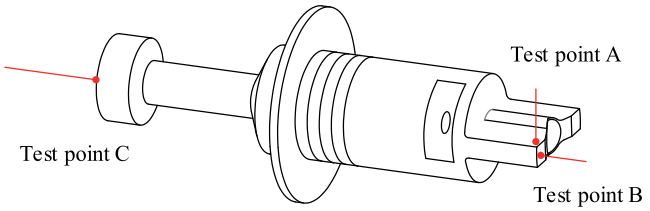

FIGURE 12. Theoretical and testing values of RPUD transducer's acoustic impedance.

rotary-percussive motion. Diameter of drill tool is 3 mm, length is 60 mm. The prototype of RPUD total length is 270 mm, and total weight is 590 g.

IV. MECHANICAL PERFORMANCE

To evaluate mechanical output performance of RPUD transducer, several experiments are carried out. A laser displacement sensor (LK-H020, KEYENCE) is used to measure vibration displacement of rotary-percussive actuator. The measuring accuracy of the laser displacement sensor is 0.02 μm. Fig. 12 shows the schematic diagram of laser displacement test. Rotary unit and percussive unit operate in resonance state after excited by resonant voltage. Vibration displacements at each test point were measured by the laser displacement sensor. Test point A and B measure torsional vibration and longitudinal vibration of V-LT coupler on rotary unit, respectively. Test point C measures longitudinal vibration of percussive horn on percussive unit.

The vibration displacements of rotary-percussive actuator are measured at the exciting voltage of 200 V under different frequencies. Test results, as shown in Fig. 13(a), show that the vibration displacement of test point A, B, and C simultaneously reach their maximum values at the same frequency 19.98 kHz, which indicates that the rotary unit and percussive unit match well with each other. The error between actual resonance frequency and theoretical frequency is only 52 Hz, which mainly caused by the difference of material parameters and simulation parameters.

Vibration displacements of test point A and B get to 16.2 μm and 8.1 μm, respectively. At the same time, vibration displacement of test point C reaches 17.7 μm. Fig. 13(b) shows the vibration displacement of test point C. Under the excitation of the sinusoidal resonant frequency, test point C on rotary-percussive composition engenders a sinusoidal vibration. The peak-to-peak value of vibration displacement is nearly 36 μm.

To further test the output performance of the transducer, the vibration displacement of the output surface of V-LT coupler and percussive horn is tested. Scatter point measurement method is adopted to obtain the vibration amplitude of transducer. The scattered point measurement method is to measure a number of points on the measuring surface, obtain the measured values at each point, and approximate the amplitude of the whole vibration surface approximately. The vibration measurement of V-LT coupler is mainly on the three

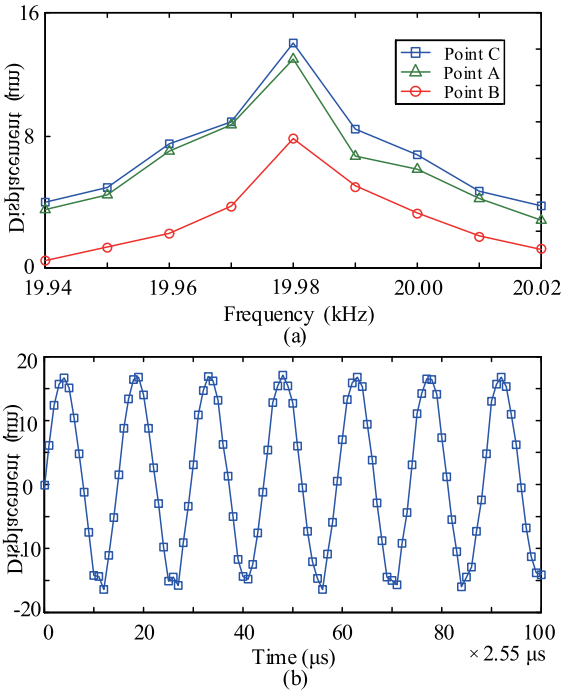

FIGURE 13. Theoretical and testing values of RPUD transducer's acoustic impedance.

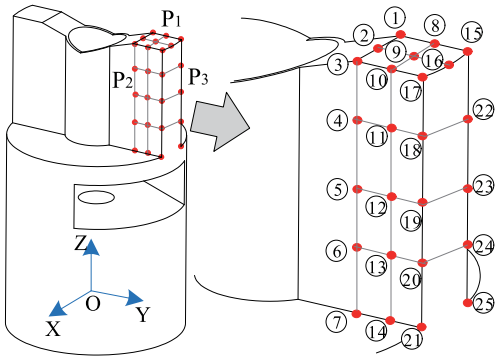

FIGURE 14. Schematic diagram of test point on V-LT coupler.

planes. As shown in Fig. 14, there are P_1 top surface which parallels to XOY surface, P_2 side surface which parallels to YOZ surface, and P_3 side surface which parallels to XOY surface.

Fig. 15(a) shows the longitudinal vibration amplitude of 9 points on the P_1 plane. It can be seen from the diagram that the longitudinal vibration amplitude of each point is nearly the same, the average amplitude of vibration amplitude is 8 μm, and the maximum deviation is about 2 μm. 20 points of P_2 and P_3 plane are selected to measure the tangential vibration amplitude of OX direction, and the vibration displacement of each point is compared. Fig. 15(b) shows that the tangential vibration of each point on the V-LT coupler driving surface increases gradually from low to upward, and the tangential vibration displacement raises with the increase

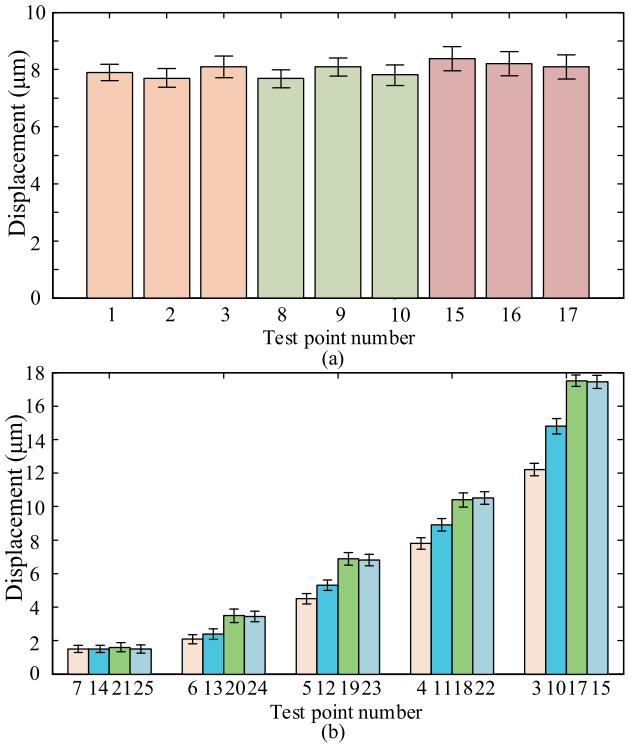

FIGURE 15. Test results of vibration displacement. (a) Vibration displacement of test points on P_1. (b) Vibration displacement of test points on P_2 and P_3.

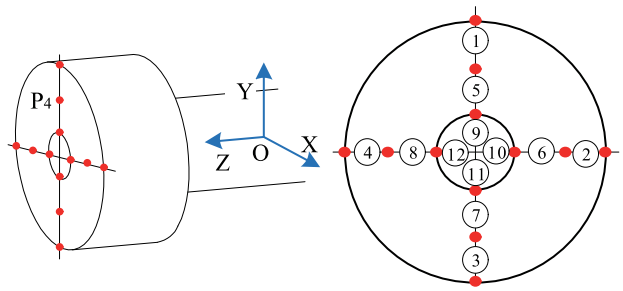

FIGURE 16. Schematic diagram of test point on percussive horn.

of the radius as well. The longitudinal vibration displacement of point 15 and point 17 at the top are the largest.

The vibration measurement of percussive horn is mainly on the P_4 plane, which is on the top driving surface paralleled to XOY surface. As shown in Fig. 16, 12 points are distributed on 3 circles with different radius. The longitudinal vibration amplitude of 12 points on the P_4 plane shows in Fig. 17. The average amplitude of vibration amplitude is nearly 18 μm, and the maximum deviation is about 2 μm. The longitudinal vibration amplitude of each point is about the same.

Based on the RPUD prototype, a rotary speed test is performed to get the optimum driving frequency. Fig. 18 shows rotary speed under different driving frequencies, while the exciting peak to peak voltage is 200 V_{PP} and preload force is 10 N. Results show that the optimum driving frequency is about 19.95 kHz. Due to the addition of drill tool and housing, the resonant frequency of RPUD is slightly lower than

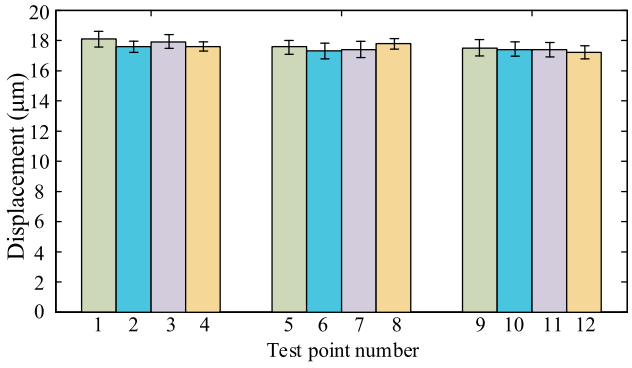

FIGURE 17. Vibration displacement of test points on P_4.

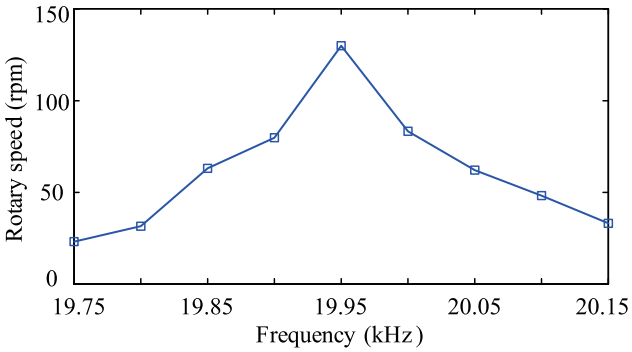

FIGURE 18. Rotary speed of RPUD under different exciting frequencies.

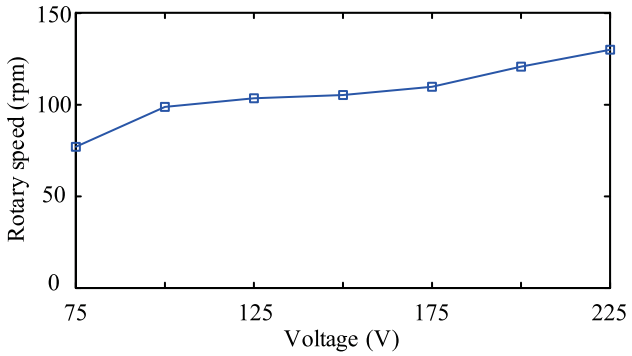

FIGURE 19. Rotary speed of RPUD under different exciting voltages.

rotary-percussive composition. Then, the driving frequency of 19.95 kHz is set as exciting frequency, and the maximum speed is measured. Fig. 19 shows that the RPUD gets the maximum speed of 117.75 rpm under exciting voltage of 225 V_{PP}. The rotary speed of the RPUD under different preload forces and driving torques is measured. As shown in Fig. 20, the maximum driving torque is 38 mNm when the preload force is 18 N (the exciting voltage is 225 V_{PP}). It can be seen that the rotary speed of RPUD has a slower decrease with a larger preload.

V. DRILLING EXPERIMENT

Based on the RPUD prototype, a test bed is built to evaluate the drilling performance, as shown in Fig. 21(a). The drilling experiments are accomplished under exciting voltage

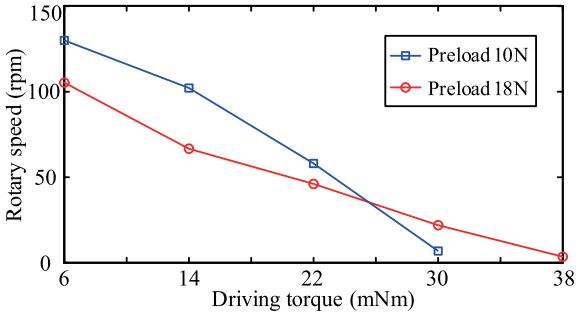

FIGURE 20. Rotary speed of RPUD under different driving torques and preload forces.

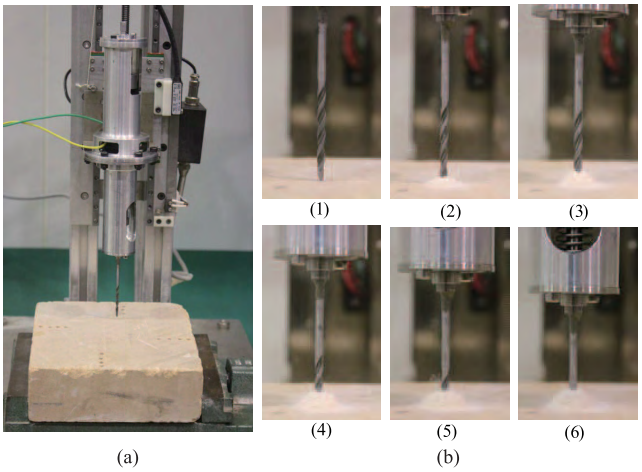

FIGURE 21. Drilling experiment of RPUD. (a) Test bed of RPUD. (b) Drilling process of RPUD on sandstone.

of 225 V_{PP} and exciting frequency of 19.95 kHz. Diameter of drill tool is 3 mm, and drilling medium is sandstone. In order to evaluate drilling ability of RPUD, a tentative drilling test is carried out, and Fig. 21(b)(1)-(6) shows the drilling process. RPUD begins to drill into sandstone, as shown in Fig. 21(b)(1). Then, Fig. 21(b)(2)-(5) shows that with the increase of drilling depth, drilling chips are removed out of drilling hole through rotary motion, which builds up a mound around drill tool. In Fig. 21(b)(6), the drilling depth of RPUD has been reached nearly 22 mm in 5 minutes. This drilling test shows that RPUD can drill into rocks and remove drilling cuttings timely.

To further evaluate the drilling capabilities of the RPUD, drilling depth under different weight on bits and free mass are measured. As shown in Fig. 22, a maximum drilling depth of 22 mm is achieved under weight on bit of 7 N. To increase the reliability of the dates, the drilling test was carried out three times. The result shows that weight on bit has a great influence on the drilling depth of RPUD. With the increase of weight on bit, the drilling depth increases firstly, then decreases gradually after reaching a peak value, which is the optimal value for the weight on bit.

Drilling depth of RPUD under different weight of free mass is shown in Fig. 23. Three experiments were conducted to

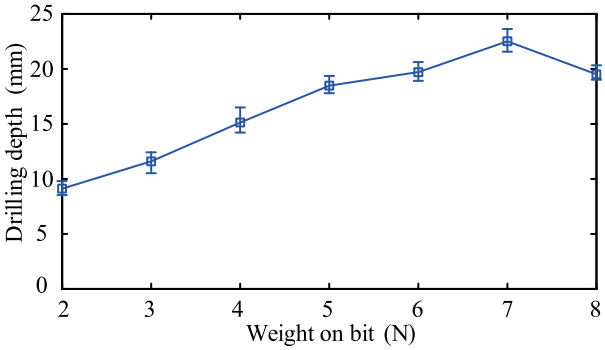

FIGURE 22. Drilling depth of RPUD under different weight on bit.

increase the reliability of the data. The drilling results shows that the drilling depth increases first and then decreases with the increase of weight of free mass. The drilling depth reaches the maximum value at the 8 g.

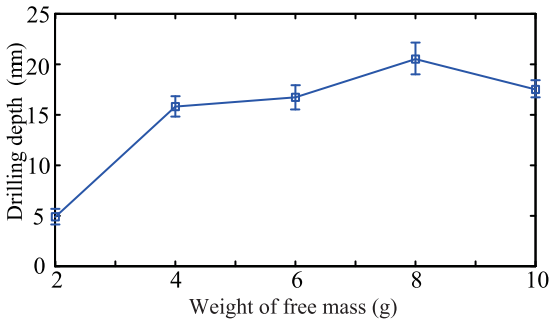

FIGURE 23. Drilling depth of RPUD under different weight on bit.

Drilling performance of rotary-percussive drilling and percussive drilling is compared. In order to keep the rationality of the experiment, percussive ultrasonic drill is represented by RPUD works at percussive mode, which removes the rotor and preload spring making no rotary motion. The compared drilling experiment was tested three times. Fig. 24 shows the contrastive drilling results. In the first minutes, there is a little difference in drilling depth between rotary-percussive drilling and percussive drilling. As drilling cuttings cannot

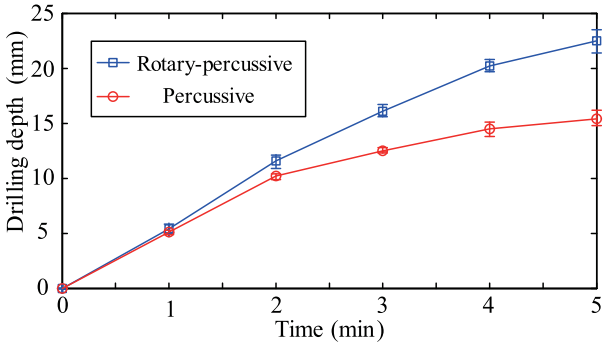

FIGURE 24. Drilling depth of RPUD under different weight on bit.

be removed timely in percussive drilling, rotary-percussive drilling gradually shows better performance after two minutes, the differences gradually increased with the increase of time. At last, drilling depth of rotary-percussive drilling is 22 mm, and percussive drilling is 15.5 mm.

TABLE 1. Comparison results between rotary-percussive drilling and percussive drilling.

Description	Rotary-percussive drilling	Percussive drilling
Weight on bit (N)	7	7
Input Voltage (V)	200	200
Maximum Power (W)	20	20
Drilling time (min)	5	5
Maximum drilling depth (mm)	22	15.5
Average drilling rate (mm/min)	4.4	3.1

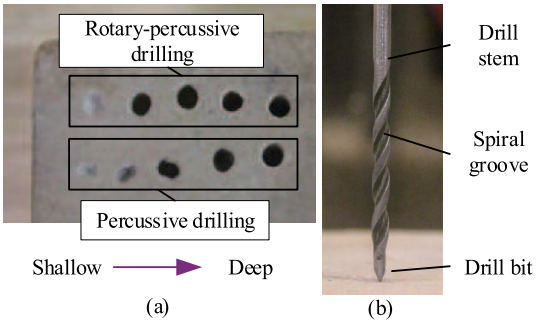

FIGURE 25. Drilling depth of RPUD under different weight on bit.

As can be seen in Table 1, maximum drilling depth and average drilling rate of rotary-percussive drilling are larger than percussive drilling. This experimental comparison demonstrates that, compared with percussive drilling, rotary-percussive drilling can remove drilling cuttings effectively, which improves drilling efficiency. The rock after one time of compared drilling experiment was chosen to show the drilling holes, as shown in Fig. 25(a). The above parts are rotary-percussive drilling holes, the below are percussive drilling holes. From left to right, the drilling time is increased by one minute. Drilling depth increases sequentially from left to right as well. As the shape of drill bit is wedge-shaped (Fig. 25(b)), the shapes of drilling holes in percussive drilling are similar to rectangle when the drilling depth is shallow. The percussive drilling holes gradually become circular after the drill bit gets to a certain depth. However, in rotary-percussive drilling, drilling holes are basically circular due to the rotary motion of drill bit.

VI. CONCLUSION

This paper proposed a Rotary-Percussive Ultrasonic Drill (RPUD) for rock sampling in minor planet exploration. RPUD is composed of piezo-ceramics, rotary unit, percussive unit, and drill tool, and driven by a single-phase electric power source. Based on the vibrations on two sides of piezo-ceramics, the RPUD achieves rotary-percussive motion of drill tool. The rotary motion and percussive motion are coupled and the working parameters can be adjusted individually. In order to realize the synchronous movement of rotary unit and percussive unit, part of parameters of the rotary-percussive actuator are adjusted to making rotary unit and percussive unit operate in resonance state under the same resonance frequency. According to the prototype of RPUD, resonance frequency and vibration displacement are measured, and the results are matched well with the finite element method. The RPUD prototype achieved rotary speed of 117.75 rpm and maximum torque of 38 mNm when the preload force is 18 N. Drilling depth of RPUD can reach to 22 mm under the weight on bit of 7 N. Contrastive experiment shows that RPUD can actually raise the drilling efficiency compared with percussive drilling. Future work will focus on the improvement of drilling capability, and reducing power consumption.

REFERENCES

[1] K. Zacny *et al.*, "Drilling systems for extraterrestrial subsurface exploration," *Astrobiology*, vol. 8, no. 3, pp. 665–706, 2008.
[2] Y. Bar-Cohen and K. Zacny, *Drilling in Extreme Environments: Penetration and Sampling on Earth and other Planets*. Weinheim, Germany: Wiley, 2008.
[3] Q. Quan, C. Chen, Z. Deng, J. Tang, and S. Jiang, "Recovery rate prediction in lunar regolith simulant drilling," *Acta Astronautica*, vol. 133, pp. 121–127, Apr. 2017.
[4] D. E. Brownlee *et al.*, "Stardust: Comet and interstellar dust sample return mission," *J. Geophys. Res., Planets*, vol. 108, no. E10, pp. SRD1-1–SRD1-15, 2003.
[5] A. Fujiwara, T. Mukai, J. Kawaguchi, and K. T. Uesugi, "Sample return mission to NEA: MUSES-C," *Adv. Space Res.*, vol. 25, no. 2, pp. 231–238, 2000.
[6] M. F. A'Hearn *et al.*, "Deep impact: Excavating comet tempel 1," *Science*, vol. 310, no. 5746, pp. 258–264, 2005.
[7] K. H. Glassmeier, H. Boehnhardt, D. Koschny, E. Kührt, and I. Richter, "The Rosetta mission: Flying towards the origin of the solar system," *Space Sci. Rev.*, vol. 128, nos. 1–4, pp. 1–21, 2007.
[8] X. Bao *et al.*, "Modeling and computer simulation of ultrasonic/sonic driller/corer (USDC)," *IEEE Trans. Ultrason., Ferroelectr., Freq. Control*, vol. 50, no. 9, pp. 1147–1160, Sep. 2003.
[9] V. N. Khmelev, V. A. Nesterov, S. S. Khmelev, D. V. Genne, S. N. Tsyganok, and V. I. Kostenko, "The development of experimental sample of ultrasonic equipment for the intake of lunar soil," in *Proc. IEEE 13th Int. Conf. Seminar Young Spec. Micro/Nanotechnol. Electron Devices*, Novosibirsk, Russia, Jul. 2012, pp. 162–169.
[10] Y. Bar-Cohen *et al.*, "Ultrasonic/sonic driller/corer (USDC) as a sampler for planetary exploration," in *Proc. Aerosp. Conf.*, Big Sky, MT, USA, Mar. 2001, pp. 1/263–1/271.
[11] P. N. H. Thomas, "Magna Parva and ESA's ultrasonic drill tool for planetary surface exploration," in *Proc. Earth Space, Eng., Sci., Construction, Oper. Challenging Environ.*, Honolulu, HI, USA, 2010, pp. 1235–1245.
[12] V. N. Khmelev, D. V. Genne, S. S. Khmelev, R. V. Barsukov, and V. I. Kostenko, "Studies of functional possibilities of model sample of the ultrasonic apparatus for drilling of the simulator of lunar soil," in *Proc. IEEE 14th Int. Conf. Seminar Young Spec. Micro/Nanotechnol. Electron Devices*, Novosibirsk, Russia, Jul. 2012, pp. 123–127.
[13] C. Potthast, J. Twiefel, and J. Wallaschek, "Modelling approaches for an ultrasonic percussion drill," *J. Sound Vib.*, vol. 308, nos. 3–5, pp. 405–417, 2007.
[14] A. Cardoni, P. Harkness, and M. Lucas, "Ultrasonic rock sampling using longitudinal-torsional vibrations," *Phys. Procedia*, vol. 3, no. 1, pp. 125–134, 2010.
[15] M. Badescu, X. Bao, Y. Bar-Cohen, Z. Chang, and S. Sherrit, "Integrated modeling of the ultrasonic/sonic drill/corer (USDC): Procedure and analysis results," *Proc. SPIE*, vol. 5764, pp. 312–324, May 2005.
[16] M. Badescu *et al.*, "Percussive augmenter of rotary drills (PARoD)," *Proc. SPIE*, vol. 8692, p. 86921Q, Apr. 2013.

[17] R. Timoney *et al.*, "The development of the European uitrasonic planetary core drill (UPCD)," in *Proc. AIAA SPACE Conf. Expo.*, Pasadena, CA, USA, 2015, pp. 1–11.
[18] K. Zacny *et al.*, "Wireline deep drill for exploration of Mars, Europa, and Enceladus," in *Proc. Aerosp. Conf.*, Big Sky, MT, USA, Mar. 2013, pp. 1–14.
[19] S. Sherrit, L. Domm, X. Bao, Y. Bar-Cohen, Z. Chang, and M. Badescu, "Single piezo-actuator rotary-hammering (SPaRH) drill," *Proc. SPIE*, vol. 8345, p. 83452B, Apr. 2012.
[20] A. Kumada, "A piezoelectric ultrasonic motor," *J. Appl. Phys.*, vol. 24, pp. 739–741, Jan. 1985.
[21] Y. Liu, X. Yang, W. Chen, and D. Xu, "A bonded-type piezoelectric actuator using the first and second bending vibration modes," *IEEE Trans. Ind. Electron.*, vol. 63, no. 3, pp. 1676–1693, Mar. 2016.
[22] Y. X. Liu, S. Shi, C. Li, W. Chen, and J. Liu, "A novel standing wave linear piezoelectric actuator using the longitudinal-bending coupling mode," *Sens. Actuators A, Phys.*, vol. 251, pp. 119–125, Nov. 2016.
[23] Y. Liu, W. Chen, X. Yang, and J. Liu, "A rotary piezoelectric actuator using the third and fourth bending vibration modes," *IEEE Trans. Ind. Electron.*, vol. 61, no. 8, pp. 4366–4373, Aug. 2014.
[24] J. Tsujino, "Ultrasonic motor using a one-dimensional longitudinal-torsional vibration converter with diagonal slits," *Smart Mater. Struct.*, vol. 7, no. 3, pp. 345–351, 1998.
[25] X. T. Tang, Y. Liu, S. Shi, W. Chen, and X. Qi, "Development of a novel ultrasonic drill using longitudinal-bending hybrid mode," *IEEE Access*, vol. 5, pp. 7362–7370, 2017.
[26] L. Xu and S. Lin, "An improved tubular ultrasonic radiator in longitudinal and radial composite vibration," *Acta Acustica United Acustica*, vol. 101, no. 1, pp. 37–45, 2015.
[27] M. Badescu, S. Sherrit, X. Bao, Y. Bar-Cohen, and B. Chen; , "Auto-Gopher: A wire-line rotary-hammer ultrasonic drill," *Proc. SPIE*, vol. 7981, p. 79813U, Apr. 2011.
[28] L. J. Vila and R. B. Malla, "Dynamic impact force on a special drilling mechanism for planetary exploration," *J. Eng. Mech.*, vol. 29, no. 4, p. 04016017, 2016.

YINCHAO WANG was born in Jining, Shandong, China, in 1985. He received the B.S. and M.S. degrees in mechanical engineering from Beihua University, China, in 2009 and 2012, respectively. He is currently pursuing the Ph.D. degree with the Harbin Institute of Technology, Harbin. His research interest is ultrasonic drilling sampling and piezoelectric actuation.

QIQUAN QUAN was born in Suzhou, Anhui, China, in 1983. He received the B.S. and M.S. degrees from the Harbin Institute of Technology, Harbin, China, in 2005 and 2007, respectively, and the Ph.D. degree from Ritsumeikan University, Japan. He is currently an Associate Professor with the State Key Laboratory of Robotics and System, Harbin Institute of Technology. His current research interest is in-orbit and on-ground testing of the aerospace mechanism.

HONGYING YU was born in Harbin, Heilongjiang, China, in 1968. She received the B.S. degrees from China Agricultural University, Beijing, China, in 1994, and the M.S. and Ph.D. degrees from the Harbin Institute of Technology, Harbin, in 1999 and 2002, respectively. She is currently a Professor with the State Key Laboratory of Robotics and System, Harbin Institute of Technology. Her current research interest is mechanical CAD and simulation technology.

DEEN BAI was born in Jining, Shandong, China, in 1987. He received the B.S. degree in mechanical engineering from Northeast Forestry University, Harbin, China, in 2011, and the M.S. degree in mechanical engineering from the Harbin Institute of Technology, Harbin, in 2014. He is currently pursuing the Ph.D. degree in mechanical engineering with the Harbin Institute of Technology. His research interests include rotary-percussive ultrasonic drills and crushing efficiency for rock.

HE LI was born in Laiwu, Shandong, China, in 1987. He received the B.S. degree in mechanical engineering from the Changchun University of Science and Technology, Changchun, China, in 2010, and the M.S. and Ph.D. degrees in mechanical engineering from the Harbin Institute of Technology, Harbin, China, in 2013 and 2018, respectively. He is currently a Lecturer with the College of Mechanical and Electronic Engineering, Shandong University of Science and Technology. His research interests include ultrasonic bearings.

ZONGQUAN DENG was born in 1956. He received the B.S. and M.S. degrees from the Harbin Institute of Technology, Harbin, China, in 1982 and 1984, respectively. He is currently a Professor with the State Key Laboratory of Robotics and System, Harbin Institute of Technology. His current research interests include special robot systems and aerospace mechanisms and control.